Annals of Biomedical Engineering, Vol. 25, pp. 964–974, 1997
Printed in the USA. All rights reserved.

0090-6964/97 $10.50 + .00

Mechanisms by which Thrombolytic Therapy Results in Nonuniform Lysis and Residual Thrombus after Reperfusion

SRIRAM ANAND* VENKAT KUDALLUR,* E. BRUCE PITMAN,† and SCOTT L. DIAMOND*

*Bioengineering Laboratory, Department of Chemical Engineering, and †Department of Mathematical Sciences, State University of New York, Buffalo, NY

Abstract—A transport-reaction model describing penetration of plasmin by diffusion and permeation into a dissolving fibrin gel was solved numerically to explore mechanisms that lead to the formation and growth of dissolution fingers through blood clots during thrombolytic therapy. Under conditions of fluid permeation driven by arterial pressures, small random spatial variations in the initial fibrin density within clots (±4 to 25% peak variations) were predicted by the simulation to result in dramatic dissolution fingers that grew in time. With *in vitro* experiments, video microscopy revealed that the shape of the proximal face of a fibrin gel, when deformed by pressure-driven permeation, led to lytic breakthrough in the center of the clot, consistent with model predictions of increased velocities in this region leading to cannulation. Computer simulation of lysis of fibrin retracted by platelets (where more permeable regions are expected in the middle of the clot due to retraction) predicted cannulation of the clot during thrombolysis. This residual, annular thrombus was predicted to lyse more slowly, because radial pressure gradients to drive inner clot permeation were quite small. In conjunction with kinetic models of systemic pharmacodynamics and plasminogen activation biochemistry, a two-dimensional transport-reaction model can facilitate the prediction of the time and causes of clot cannulation, poor reperfusion, and embolism during thrombolysis.

Keywords—Thrombolysis, Plasmin, Fibrin, Diffusion, Embolism.

INTRODUCTION

The treatment of arterial and venous thrombi with thrombolytic agents can often result in partial reperfusion via dissolution fingering where residual and potentially thrombogenic material is left on the vessel wall. These annular clots are likely prone to reocclusion. The creation of partially occluding, residual thrombi during thrombolytic therapy may be the result of arterial pressures driving fluid permeation nonuniformly through interstitial regions of the clot matrix. The effects of pressure-driven fluid permeation on thrombolysis have been characterized *in vitro* with purified fibrin gels, whole blood clots, and retracted blood clots (2,3,4,7,19). *In vivo* studies have also demonstrated the enhancing effects of pressure-driven permeation during thrombolysis where transport and thrombolysis were reduced under conditions of cardiogenic shock or hypotension (9,15). Since the lysis of thrombi involves complex spatial dynamics of numerous reactions coupled with diffusive and pressure-driven permeation (2,7) in conjunction with prevailing systemic pharmacodynamics (1,18), the initial clot structure will likely play an important role in lytic outcomes, such as partial reperfusion or reocclusion.

In previous studies, we have used a one-dimensional model to predict the rate of progression of a lysis front based on local and intravenous delivery of lytic agents (1,2,7). This approach has been tested against *in vitro* experiments using plasmin, urokinase (uPA), and tissue plasminogen activator (tPA), and extended to account for solubilization of fibrin-bound species for renewed rounds of reaction (2), as well as to account for pharmacodynamics of intravenous delivery (1). Thrombolysis, however, occurs on clots of complex structure that have been formed dynamically under complex flow conditions. These structures can lyse nonuniformly with lytic breakthrough a common outcome (3,5). The goal of the present study was to explore the mechanisms by which highly nonuniform lysis (*i.e.*, dissolution fingering) occurs.

THEORY

To explore lysis front dynamics (shape and velocity) as fibrin is eroded by pressure-driven permeation of a reactive and binding fibrinolytic mediator, we have formulated a two-dimensional convection-diffusion model that ac-

Acknowledgment—The authors acknowledge the State University of New York School of Engineering and Applied Sciences for use of the SUN SparcCenter 2000 machine, as well as the National Science Foundation Instrumentation Grant CTS 9212682 (T.J.M.) for use of a SGI R4000 computer. This work was supported by the National American Heart Association Grant 96-6670 (S.L.D.), National Institutes of Health Grant R01HL56621 (S.L.D.), and Grant DMS 9504433 (E.B.P.). S.L.D. is the recipient of the National Science Foundation National Young Investigator Award.

Address correspondence to Scott L. Diamond, Institute for Medicine and Engineering, Department of Chemical Engineering, 394 Towne Building, 220 South 33rd Street, University of Pennsylvania, Philadelphia, PA 19104-6393, U.S.A.

(Received 18Dec96, Revised 26Feb97, Revised, Accepted 7Mar97)

counts for changing species concentration in the fluid phase and fibrin fiber phase of an erodible clot. Since the biochemical complexity that had been obtainable in prior one-dimensional models (2,7) is computationally prohibitive for two-dimensional problems, we have treated the case of pressure-driven permeation of plasmin into fibrin structures of arbitrary structural complexity. Understanding the dynamics of lysis front progression for plasmin-mediated fibrinolysis is a first step toward evaluating more complex biochemical situations.

The rate of change of plasmin concentration **c** at any position in the fluid of the dissolving clot is given by Eq. 1, where the velocity field $\mathbf{v}(x,y,t)$ of the permeating fluid is continually changing due to changes in fibrin permeability during lysis (2,7). The net rate of change of the fibrin-bound plasmin concentrations **s** is the sum of the adsorption rate and desorption rate (Eq. 2) for plasmin binding to a fixed number of sites (θ) in fibrin (7). The adsorption step is relatively fast, compared with the desorption step and may rapidly approach a high degree of binding equilibrium. The desorption step may often be in states of nonequilibrium for certain reaction or transport conditions that deplete the fluid phase concentration of plasmin (7). We take the forward rate of binding of plasmin to fibrin to be on the order of 0.5×10^{-3} μM^{-1} sec^{-1}, which provides for plasmin adsorption to approach equilibrium within several seconds. Under conditions of rapid fibrinolysis, the return of plasmin to the fluid phase more often involves a kinetic step (solubilization) that is typically more rapid than desorption reequilibration (2). Homogeneous reactions (**R** in Eq. 1) for plasmin include plasmin autoproteolysis and α_2-antiplasmin inhibition, but these reactions were not treated in the present study. Parameters are given in Table 1.

$$\underset{\text{rate of change of c}}{\varepsilon \frac{\partial \mathbf{c}}{\partial \mathbf{t}}} = \underset{\text{gain due to lysis}}{(\mathbf{s}-\mathbf{c})\frac{\partial \varepsilon}{\partial \mathbf{t}}} - \underset{\text{net adsorption to fibrin}}{(\mathbf{1}-\varepsilon)\frac{\partial \mathbf{s}}{\partial \mathbf{t}}} + \underset{\text{diffusion/dispersion}}{\nabla \cdot (\mathbf{D} \cdot \nabla(\varepsilon \mathbf{c}))} - \underset{\text{permeation}}{\nabla \cdot (\varepsilon \mathbf{c} \mathbf{v})} + \underset{\text{homogeneous reaction}}{\varepsilon \mathbf{R}} \quad (1)$$

$$\frac{\partial \mathbf{s}}{\partial \mathbf{t}} = \underset{\text{adsorption}}{\mathbf{k_f}\, \mathbf{c}(\theta - \mathbf{s})} - \underset{\text{desorption}}{\mathbf{k_r}\, \mathbf{s}}. \quad (2)$$

We imposed an upstream pressure on the proximal face of the clot at x = 0 and y = 1 cm). The superficial permeation velocity $\bar{\mathbf{v}}$ through the porous fibrin matrix of the blood clot is given by Darcy's law (Eq. 3) for plasma of viscosity μ permeating through fibrin with a specific permeability **k.**

$$\bar{\mathbf{v}} = -\mathbf{K} \nabla \mathbf{P} \text{ where } \mathbf{K} = \mathbf{k}(x,y,t)/\mu. \quad (3)$$

To calculate $\bar{\mathbf{v}}_x$ and $\bar{\mathbf{v}}_y$ at every position and time, the Poisson equation (Eq. 4) is solved with the complication that the hydraulic permeability (**K**) is varying in space and time due to lysis. The specific permeability depends directly on the local fiber diameter $\mathbf{D_{fiber}}(x,y,t)$ and fibrin gel porosity $\varepsilon(x,y,t)$. The specific permeability is suitably correlated (7) with the fiber diameter and the fibrin porosity by the Davies equation (8), where $\mathbf{k} = \mathbf{D}^2_{\mathbf{fiber}}/(70(1-\varepsilon)^{3/2}\{1 + 52(1-\varepsilon)^{3/2}\})$. The initial permeability field $\mathbf{k}(x,y,t = 0)$ was set as described in Appendix I.

$$\nabla \cdot \bar{\mathbf{v}} = \nabla \cdot (\mathbf{K}(x,y,t) \nabla \mathbf{P}) = 0. \quad (4)$$

In eroding fibrin, it is necessary to relate the evolving material properties (fiber diameter and local permeability) with the proteolysis rate. By evaluating at all times the instantaneous rate of cutting within the fiber $\{k_{cat} \cdot s_{plasmin}$, ($\mu$mol/l)/sec$\}$ at some location x', it is possible to calculate the historic amount of cutting within the fiber {μmol/l of cleavages} made at x′ and t′. The solubilization factor γ relates the number of equivalent monomers solubilized to the number of cleavages made such that the amount of solubilization or lysis {(L(x′,t′), μmol/l of fibrin lyzed at x′ and t′} from the solid phase can be defined as a function of the historic amount of cuts made by plasmin at position x′ (Eq. 5). For fibrin, the solubilization factor has been set to 0.1 corresponding to the estimate that, for every 10 cleavages by plasmin, an equivalent of one subunit of fibrin is solubilized (16).

$$\mathbf{L(x',t')} = \gamma \int_0^{t'} \mathbf{k_{cat}}\, \mathbf{s_{plasmin}(x',t)}\, \mathbf{dt}. \quad (5)$$

TABLE 1. Model parameters for biochemical and transport processes for plasmin-mediated fibrin lysis (2,7).

Dissociation constant (K_d)	0.5 μmol/l
Forward association rate (k_f)	0.5×10^{-3} μmol/l^{-1} sec^{-1}
Reverse dissociation rate (k_r)	10^{-3} sec^{-1}
Fibrin cleavage rate by bound plasmin (k_{cat})	5 sec^{-1}
Monomers released per cleavage event (γ)	0.1
Effective diffusion coefficient (D)	5×10^{-7} cm^2/sec
Longitudinal dispersion coefficient ($\mathbf{D_L}$)	$\mathbf{D_L} = D + 1.0\ (\mathbf{D_{pore}})\ \mathbf{v_x}$
Transverse dispersion coefficient ($\mathbf{D_T}$)	$\mathbf{D_T} = D + 0.1\ (\mathbf{D_{pore}})\ \mathbf{v_y}$
Pressure drop (ΔP)	50 mm Hg
Initial clot length (L)	1 cm
Thrombi fibrin density	220 μmol/l
Fiber radius (R_f)	250 nm

The local plasmin concentration in the fiber and the solubilization rate are formulated with respect to a volume average within the solid fiber volume. Plasmin gradients within the fiber are not calculated. Calculation of the fiber properties during lysis were conducted as previously described (2,7). Briefly, to quantify the change in fibrin fiber volume upon lysis, the total length of fibers initially in the gel (L_T/V_t) was first calculated from the uniform initial radius R_{fo}, fibrin fiber density (ρ_{fiber}), initial gel density (ρ_o), and total clot volume, V_T. The local dynamic change in fibrin gel porosity (ε) was related to the local extent of lysis **L** by allowing the radius of the fibers R_f to shrink at constant fibrin fiber density (ρ_{fiber} = 0.28 g/ml-fiber and $s_o = \rho_{fiber}/MW_{monomer}$):

$$\mathbf{R_f(x,t)^2 = (R_{fo}^2) \cdot \frac{s_o - L(x,t)}{s_o}}. \tag{6}$$

For an initial fiber radius R_{ro} and a total fiber length density L_T/V_T, the initial gel porosity is:

$$\varepsilon_o = 1 - \pi \mathbf{R_{fo}^2 (L_T/V_T)\ 10^{-21}\ cm^3/nm^3} = 1 - (\rho_o/\rho_{fiber}). \tag{7}$$

The local instantaneous porosity $\varepsilon(x,t)$ based on the local instantaneous fiber radius $R_f(x,t)$ is calculated similarly. The percentage of lysis is then known at any position by:

$$\mathbf{\%\ Lysis(x,t) = \left[1 - \left(\frac{R_f(x,t)}{R_{fo}}\right)^2\right] \cdot 100 = \frac{L(x,t)}{s_o} \cdot 100.} \tag{8}$$

The fibrin density and porosity change at each position and time as the structure is dissolved. This has important consequences on fluid phase level of plasmin due to solubilization. However, spatial gradients in porosity and dispersion do not serve as a driving force for diffusion or convection. Therefore, to simplify the solution of Eq. 1 for transport and reaction in two dimensions, first and second spatial derivatives of **D** and ε were neglected. This assumption is valid proximal and distal to the lysis front and only breaks down in the thin region of the lysis front where gradients in the material properties may be significant. Also, expansion of the expression for permeation in Eq. 1 results in the term $\nabla \cdot \mathbf{v}$, which was neglected since the term was small throughout the domain. These simplifications result in over 10 derivatives being dropped from the governing equation (a considerable computational savings), with no essential physics lost from the problem, at a cost of small deviations in the conservation of mass only at the lysis front. In comparison with one-dimensional simulations (2) that include all spatial derivatives of **D** and ε, the neglect of these derivatives produces less than a 3% loss of mass over the entire reaction domain (see *Results*). In two dimensions, the dispersion and permeation terms of Eq. 1 are thus simplified as follows where the transverse dispersion coefficient (D_T) in the radial direction and the longitudinal dispersion coefficient in the axial direction (D_L) are defined in Table 1 to be the sum of Brownian diffusion and hydrodynamic micromixing:

$$\nabla \cdot (D \cdot \nabla(\varepsilon\, c)) \cong \varepsilon \nabla \cdot D \cdot \nabla(c) = \varepsilon\, D_L \frac{\partial^2 c}{\partial x^2} + \varepsilon\, D_T \frac{\partial^2 c}{\partial y^2} \tag{9}$$

$$\nabla \cdot (\varepsilon\, \mathbf{c}\, \mathbf{v}) \cong \varepsilon\, \mathbf{v_x} \frac{\partial c}{\partial \mathbf{x}} + \varepsilon\, \mathbf{v_y} \frac{\partial \mathbf{c}}{\partial \mathbf{y}} = \bar{\mathbf{v}}_\mathbf{x} \frac{\partial \mathbf{c}}{\partial \mathbf{x}} + \bar{\mathbf{v}}_\mathbf{y} \frac{\partial \mathbf{c}}{\partial \mathbf{y}}. \tag{10}$$

Numerical Solution

Evaluation of the plasmin concentration at every point in the domain requires that the velocity field be known at all times. To discretize the equations for the finite differences method, a staggered grid was used for the solution of the pressure field. The pressure was defined at the edges of the 9-point computational stencil and the velocity, permeability, and plasmin concentration were defined at the center of each cell block. The grid for discretization is described further in Appendix II. Discretization of Eq. 4 resulting from the enforcement of the zero divergence condition gave a single equation involving the x- and y-directed components of the superficial velocity at each node in the domain. Assembling these equations in matrix form, a sparse matrix was obtained with 9 nonzero bands. The public domain package *nspcg* (Non-Symmetric Preconditioned Conjugate Gradient solver, obtained from the netlib repository) uses a preconditioned conjugate gradient algorithm to solve the sparse matrix and was found to be robust even when the permeability values were changing rapidly in time and space. The point Jacobi method was used as the preconditioner with the Orthomin method (11,14) serving as the accelerator. The package typically needed $O(N^2)$ iterations to converge for the first time step and needed only a few iterations for subsequent time steps, except under conditions of robust lysis when the permeability field was changing rapidly. Once convergence was obtained to yield the pressure field within the clot, the superficial velocity field was calculated using a discretization of the gradient of the pressure (Eq. 3).

The algorithm to solve the plasmin concentration profile is similar to that formulated by LeVeque (12). Equation 1 has an advective (permeation) part, a dispersive part, and a source part that includes homogeneous reaction, solubilization from the bound phase, and reversible adsorption. To suitably resolve the different time scales in the problem, Strang splitting was used (17). For each time step, the advective part was solved using the LeVeque scheme for a half time step. Then, the diffusion part and the source part were solved using an implicit procedure for a full time step with the advective part once again solved

for a final half time step to yield the solution at the new time level. The scheme is a variant of the Lax-Wendroff method and involves a novel treatment of the cross-derivative terms arising in multidimensional modeling. This scheme uses an upwind formulation to resolve the cross-derivatives and hence was significantly more stable than the centered scheme used in the conventional Lax-Wendroff method (6,12).

The inclusion of the source part during Strang splitting deserves special mention because it involves a term that accounts for the solubilization of the bound plasmin from dissolving regions of the solid phase. A Crank-Nicholson scheme was used to discretize the diffusive part and source part of Eq. 1, which represent the contribution to the concentration of the species due to nonadvective effects. Using a Crank-Nicholson scheme, the equation was discretized by using second-order, accurate-centered differences in space at any time level t. Centered differences were used for the time derivatives at time level t + ½. Subsequently, the source part was evaluated implicitly, and the coefficients were lumped with the unknown coefficients of the concentrations at time level t + 1. This resulting discretized and assembled set of equations produced a sparse matrix with five nonzero bands. The solution of this matrix was obtained by using the *nspcg* package as before. Upon convergence, the solution of these intermediate values was passed to the advective algorithm for further refinement to obtain the free phase concentration values at the t + 1 level. It should be noted that, because of the low values of the diffusivity of proteins in water (5.0×10^{-7} cm^2/sec) and low dispersivity of fibrin (small pore diameter), the system obtained with the Crank-Nicholson scheme was diagonally dominant and the solution could effectively be obtained by explicit inversion. However, the *nspcg* algorithm was used to ensure robustness for systems where the diagonal dominance might not be so pronounced.

Subsequent to the solution of the free phase plasmin concentration, the bound fiber phase concentration was calculated to compute the local lysis rate. Due to the direct coupling between the free and bound phase concentrations and the complexity in simultaneous solution of Eqs. 1 and 2, we obtained the bound phase concentration separately. This was accomplished by an implicit procedure. A preliminary guess for the bound phase values at the time level t + ½ was obtained by an implicit formulation from Eq. 1. A simple average of this value and the value of the concentration at the time level t was obtained, and this average was used for the calculation of the free phase concentration by the Strang splitting procedure. The updated value of the free phase concentration at the time level t + 1 was used to obtain the new bound phase concentration by a fully implicit solution of Eq. 1. The updated value of the bound phase concentration of the species at the time level t + 1 was used to compute the degree of lysis of the solid phase as previously described (2). The calculation of the percent lysis resulted in the calculation of the new porosity and permeability in each cell block. The new permeability values were then used to obtain the velocity field for the next time step.

MATERIALS AND METHODS

Purified human thrombin was obtained from Sigma Chemical Co. (St. Louis, MO, USA) as a lyophilized powder (specific activity: 3,000 NIH U/mg). Lyophilized human fibrinogen (Grade L, Kabi AB) was dissolved in 0.05 M Tris-HCl (pH 7.4), dialyzed, centrifuged, and the supernatant was frozen in small aliquots at −75°C. Purified human plasmin (American Diagnostica, Inc., Greenwich, CT, USA) was reconstituted, centrifuged, and stored at −75°C. Purified fibrin gels (2 cm long) were formed by prompt suction pipetting within 15 sec of a rapidly mixed solution of fibrinogen (3 mg/ml) and thrombin (1 U/ml) into 100 μl glass capillary tubes (1.5 mm diameter). The buffer for fibrin polymerization was 0.05 M Tris-HCl, 5 mM $CaCl_2$ (pH 7.4), with 0.1 M NaCl to obtain turbid coarse gels. The clots were then perfused with 0.05 M Tris-HCl buffer using a Harvard Apparatus Syringe Infusion Pump 22 that allowed the permeation velocity to be maintained constant in a range from 0.1 to 1.0 mm/min. Permeation and lysis experiments were recorded with a CCD72 (Dage-MTI) videocamera, through a Nikon microscope with a Nikon 4× lens (PhL, 0.13 DL) with real-time digital contrast enhancement using an Argus 10 image processor (Hamamatsu Corp., Bridgewater, NJ, USA).

RESULTS

Comparison with One-Dimensional Model

The predictions of the model presented here were compared with the calculations of the one-dimensional model previously described (2) that contained all spatial derivations of **D** and ε. The comparison with the one-dimensional result was conducted to examine the effect of neglecting these derivatives in Eqs. 9 and 10. These comparisons were conducted under conditions where the fibrin had uniform density and the lysis front was completely planar. In the simulation, a pressure gradient of 50 mm Hg/cm clot was applied across a compacted fibrin clot (220 μmol/l fibrin of coarse fibers of 250 nm radius) of 1 cm length and uniform permeability of 3.16×10^{-11} cm^2. Lysis was accomplished by the infusion of 1 μmol/l of plasmin. In Fig. 1, we present the lysis profiles after 30 min. The predictions of the two-dimensional model were consistent with the one-dimensional calculations. In fact, the algorithm used to update the plasmin concentration (12) had slightly less numerical dispersion than the cen-

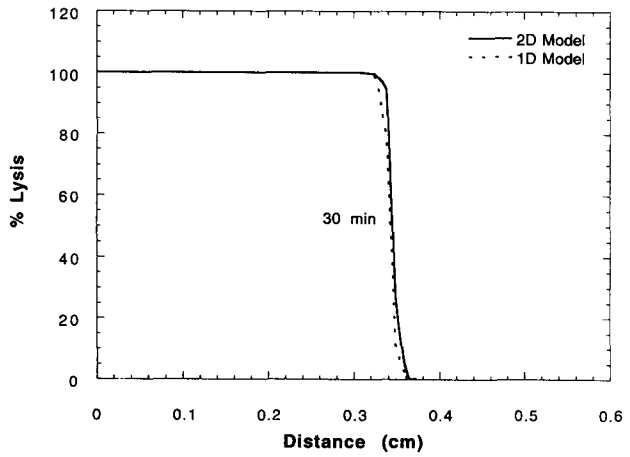

FIGURE 1. Comparison of lysis profiles at 30 min for a one-dimensional model (5) (1D; dashed line) and a two-dimensional model (2D; solid line) for continuous infusion of 1 μmol/l plasmin into a coarse, compacted clot (220 μmol/l fibrin, 250 nm fiber radius) of uniform properties under a pressure gradient of 50 mm Hg/cm clot. Flow is from left to right.

tered difference scheme used previously (2,7). Hence, this method captures the front position more sharply for a given mesh resolution. We found that both the schemes conserved mass to a satisfactory extent (within 3%). Since there were no gradients in the y direction for the two-dimensional model, the percent lysis profile is presented at y = 0.5 and was equivalent to all profiles at any value of y across the width of the clot.

The formation and growth of dissolution fingers was a motivating factor in the extension of the one-dimensional model to two dimensions. The development of dissolution fingers in blood clots undergoing thrombolysis is relevant to the creation of residual nonoccluding thrombi with low-grade reperfusion and embolism. In the following calculations, the position of the lysis front was taken as the leading location that achieved 50% lysis (*e.g.*, at ~0.35 cm in Fig. 1). Permeation and lysis proceeded from left to right in all simulations and figures.

Spatial Variability of Initial Fibrin Density

In concert with platelet activation/aggregation, a blood clot is formed dynamically under flow by the polymerization of fibrin monomers into protofibrils with subsequent aggregation of these protofibrils into thick bundles. The orientation and density of these fibers in the fibrin and consequently the clot porosity can vary considerably within the clot. To simulate this effect, a porous bed was defined by randomly generating the fibrin density at each cell in the domain subject to a random but bounded fluctuation about a mean value (Appendix I). This fibrin density was then used to calculate the porosity at each location in the domain that then allowed calculation of the local permeability. The pattern of variation of the permeability was dependent on the random generation of the density and hence on the seed used to generate the specific random number for each cell. The velocity field obtained was dependent directly on the nature of the permeability field and hence a given seed resulted in a specific velocity field. Initially, the velocity field was largely x-directed with small y-directed fluctuations due to the random nature of the media. Figure 2 shows lysis profiles with time for three different fibrin gels that all had a maximum variation of ±13.7% in the permeability around a baseline permeability of 3.16×10^{-11} cm^2 (corresponding to peak fluctuations in

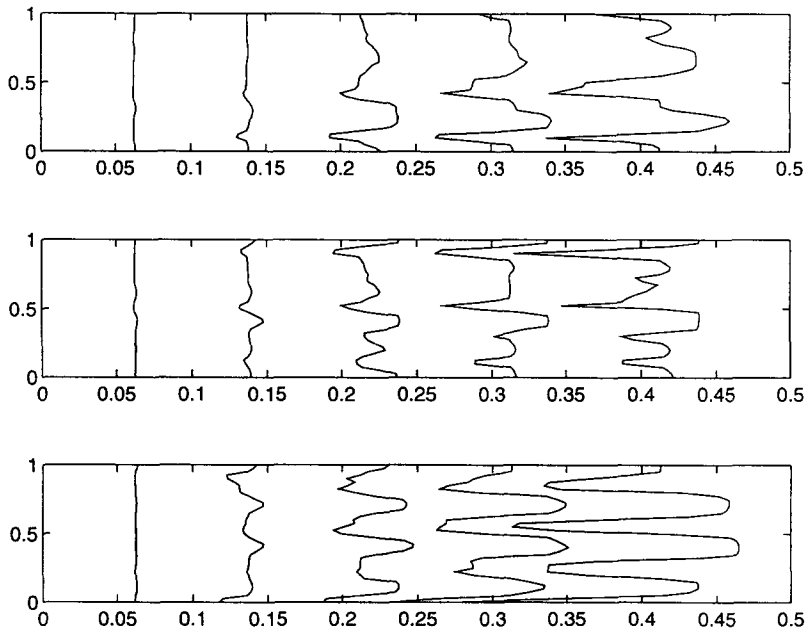

FIGURE 2. Lysis front position at various times for lysis mediated by 1 μmol/l plasmin under the conditions of Fig. 1 for fibrin domains containing an initial maximum variation in fibrin density of ~4% (peak variation in permeability of 13.7%). Panels show the lysis front position at 10-min intervals ranging from 20 to 60 min for initial fibrin domains generated using different seeds for the random number generator.

fibrin density of only ±4%), but were created with different random number generator seeds. The plasmin concentration profiles and the lysis front shape revealed that the fingers progressed fastest in regions where the initial permeability was highest and therefore provided for enhanced plasmin transport. As a given region was lysed, the porosity in this region increased to 1.0, resulting in the region being highly permeable (maximum **k** limited numerically to 10^{-9} cm^2), compared with nearby regions that were not fully lysed (**k** ~ 10^{-11} cm^2). Therefore, small differences in front position at early times were enhanced and magnified as lysis proceeded. For the three random fibrin gels shown in Fig. 2, the mean finger length increased with time for the three different clots to a length of ~1 mm by 60 min for gels with a maximum variation in permeability of ±13.7%.

To study further the effect of statistical randomness, we increased the magnitude of the peak variation of the initial fibrin density without changing the seed of the random number generator. Increasing the variability of the initial fibrin density resulted in increasing the size of the lytic fingers. In Fig. 3, we show the lysis front at various times for increasing maximum fibrin density variation from 4% to 25%. In Fig. 3A–C, the mean variation in fibrin density ranged from 2 to 13%, and the mean variation in permeability ranged from 7.2 to 49.65%. The maximum variation in permeability ranged from 16.9 to 86%. The depth of penetration of the dissolution fingers increased dramatically with increase in the variability of the permeability field. Spatial variations in the initial density of the fibrin can thus dictate the pattern of lysis and resulting lytic breakthrough with consequent early, but low-grade reperfusion. As fluid velocities increased at the tip of the finger where the pressure gradient was highest, plasmin also continuously accumulated at the lytic finger tip.

Platelet Retraction on Initial Spatial Variation of Fibrin Density

Platelets have an important role in clot mechanics and in the biochemistry of fibrinolysis. Apart from their role in the secretion of inhibitors like plasminogen activator inhibitor-1, they can regulate the structural nature of a blood clot. Through RGD-dependent interactions between glycoprotein IIb/IIIa and fibrin, the platelets can retract the fibers leading to a significant reduction in clot porosity and a concomitant rise in fibrin density. We hypothesize that a possible effect of this retraction is that some fibers of fibrin would be pulled toward the walls of the vessel leaving a less dense region in the middle of the clot. During isotropic retraction of a whole blood clot bounded by a rigid boundary (diseased vessel wall), the isometric stress generated by the platelets would be alleviated by any defects in the fibrin, thus causing retraction of the fibers towards the wall. It is hypothesized that this platelet-mediated retraction might be one mechanism by which the core of a blood clot lyses faster and gives breakthrough as observed by others (3,5). The effect of platelet retraction was simulated by generating a random fiber density biased such that it had lower fiber density (by 12%) in the middle of the clot relative to the fibrin near the walls. This resulted in higher velocities and faster delivery of plasmin to

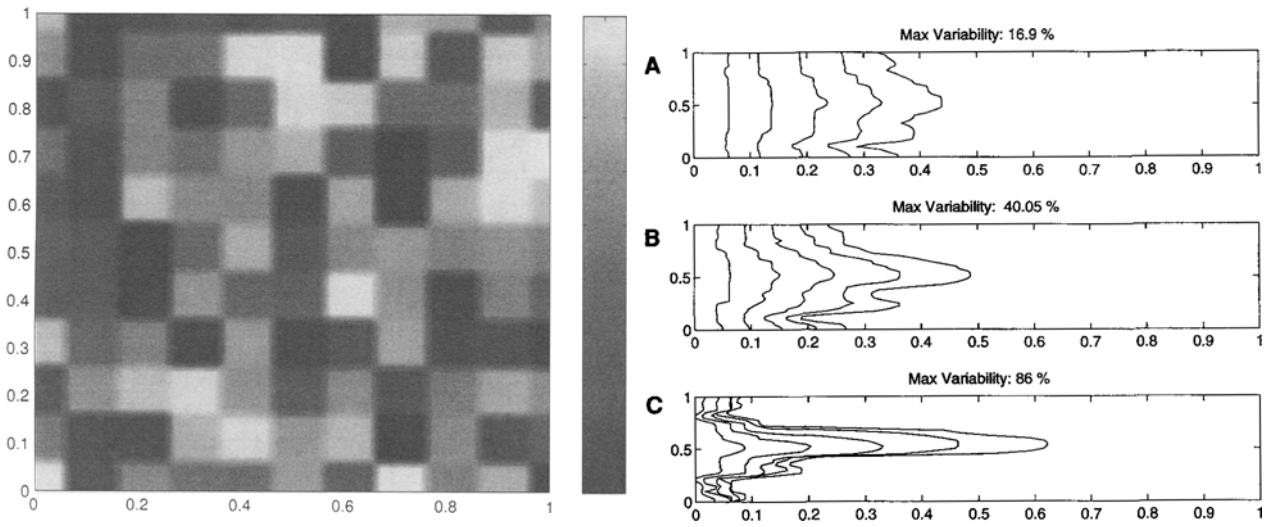

FIGURE 3. Lysis front progression at 10-min intervals ranging from 20 to 60 min for fibrin beds of increasing variability in local fibrin density and permeability. The initial permeability field had random variations in permeability around a baseline value (mid-gray) of 3.16 × 10^{-11} cm^2 (top). All gels had the same mean permeability. Lysis simulations (A–C, bottom) conducted under the conditions described in Fig. 1. For fibrin with a maximum variation in permeability of 16.9% (mean variation: 7.2%) associated with a 4% maximum variation in fibrin density, lysis fronts are given (A). For fibrin with a maximum variation in permeability of 40.05% (mean variation: 21.25%) associated with 15% maximum variation of fibrin density, lysis fronts are given (B). For fibrin with maximum variation in permeability of 86% (mean variation: 49.65%) associated with a 25% maximum variation of fibrin density, lysis fronts are given (C). The seed used for the random number generator was set constant (−1,957) for all cases.

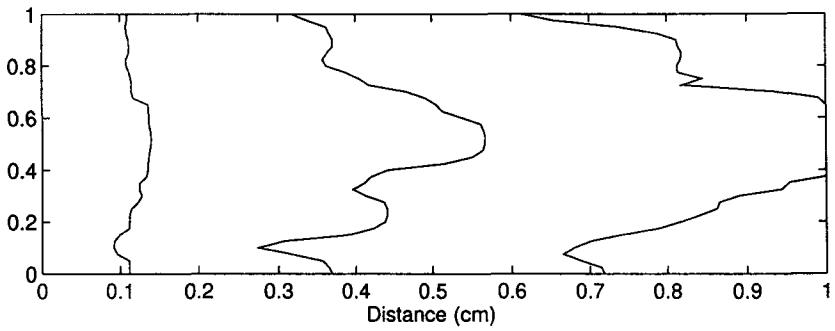

FIGURE 4. Lysis front positions for a platelet retracted clot. Lysis front positions are indicated at 20, 30, and 60 min for conditions described in Fig. 1. The initial fibrin density was calculated by generating a random number biased by a Gaussian function to generate lower fibrin density values in the middle of the clot (see Appendix I). This density distribution was then used to compute the initial permeability distribution, which was highest in the middle of the clot on average.

the middle of the clot, and consequently this region of the clot dissolved faster (Fig. 4).

Deformation of Proximal Face of Occluding Thrombi by Pressure-Driven Permeation

A rheological mechanism that may result in higher velocities in the middle of the clot is the deformation of the inlet face of the clot when subjected to arterial pressures. Under *in vitro* conditions, pressure-driven flow deformed the proximal face of the clot owing to the drag force exerted on the fibrin fibers by the flow and the firm attachment of fibrin to the walls of the tube. This mechanism is illustrated in Fig. 5A,B, which shows video images of the fibrin gel before and after permeation had been established without plasmin. The inlet of the clot was deformed, thus causing a slightly higher fluid flow into the middle of the clot. In these experiments with fibrin gels, the maximum deflection of the inlet face was found to be on the order of 0.2 mm for a superficial velocity of 0.5 mm/min. The deformed inlet appears to act as a narrowing porous-walled "tube" to direct flow into the center of the gel. We have also observed fluorescent proteins (plasmin and albumin) entering faster into the center of the gel. Although we do not simulate viscous flow into a deformable porous media, a simulation to explore the role of elevated velocities in the center of the clot can be run using a deformed inlet of the clot that has constant fibrin density.

To explore the effects of this complex rheological phenomenon via computer simulation, a Gaussian with maximum deflexion of 0.5 mm was used for the inlet of the clot to approximate the shape seen in Fig. 5B. Consistent with *in vitro* experimental observations of nonplanar lysis fronts at high permeation velocity (Fig. 5C), the core of the clot was predicted to lyse significantly faster due to the initial elevation of the velocity in the center core of the clot (Fig. 6A). In the experiment, the fibrinogen was polymerized to form a highly uniform structure that did not display small scale lytic fingering. Thus, the initial shape of the proximal face of the clot may be important in regulating the time of lytic breakthrough (reperfusion).

Lytic Rate of Annular Clots After Initial Lytic Breakthrough

By a variety of mechanisms discussed, unlysed fibrin can remain on the vessel walls after lytic breakthrough in the core of the clot. These residual thrombi would be expected to lyse slowly owing to the lack of inner clot permeation through these structures. Lysis would occur predominantly by radial diffusion mechanisms. To illustrate this transition in overall clot lysis rate that occurs after reperfusion, we present in Fig. 6B a plot of the average global lysis with time for the simulation shown in Fig. 6A. The rate of lysis remains relatively constant for ~60 min, but slowed rather abruptly once reperfusion had been achieved. This indicated that under permeation conditions, low grade perfusion might be achieved early (in 45 to 60 min), but the slow dissolution of the clot on the walls would require a substantially longer time for complete

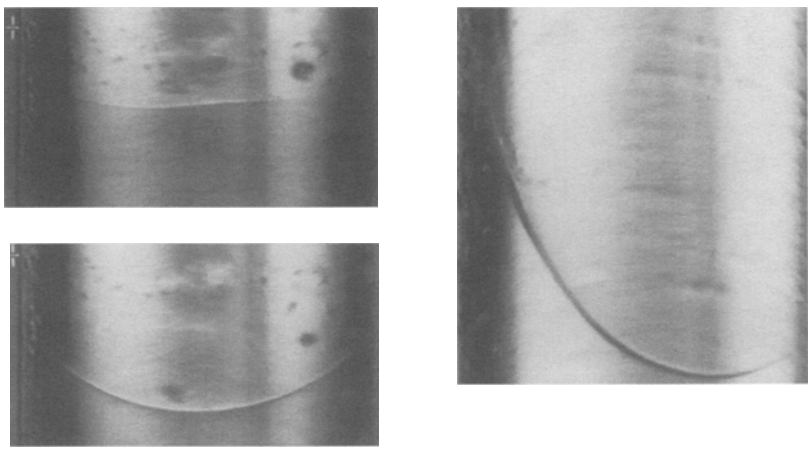

FIGURE 5. Shape of the inlet face of a fibrin clot under no flow conditions (A) or subjected to permeation of buffer (no plasmin) at a superficial velocity of 0.5 mm/min (B). Permeation is from top to bottom. The lysis front displayed substantial deviation from a planar geometry upon infusion of 1 μmol/l plasmin (C).

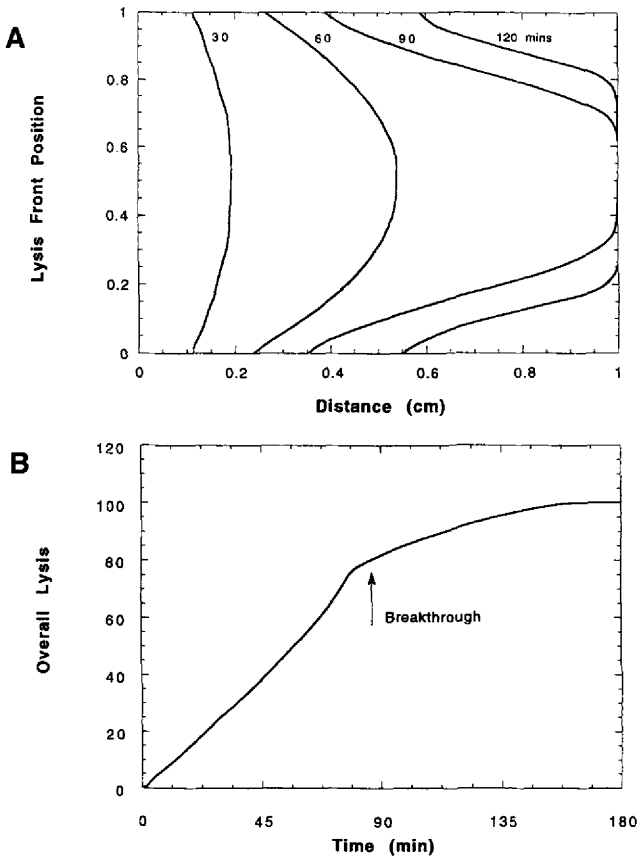

FIGURE 6. Simulation of lysis front position from 30 to 120 min and overall lysis for a clot with an initially deformed inlet face of 0.5 mm similar to the one seen in Fig. 5B (A). The overall clot lysis with time is calculated as the amount of lysis occurring over the entire clot domain (B).

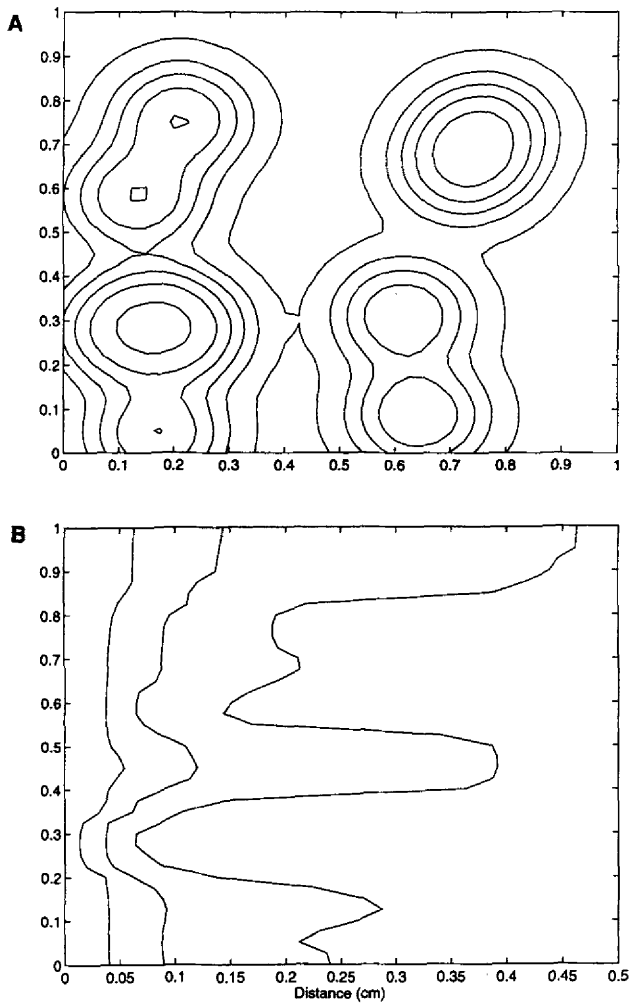

FIGURE 7. Simulation of lysis front propagation in a clot with seven, variably sized clumps of high fibrin density (low permeability of 0.5×10^{-11} cm^2 in the center of each clump) in a uniform domain with permeability of $k = 3.16 \times 10^{-11}$ cm^2. The initial fibrin density was generated as described in Appendix I, and the resulting permeability field is shown in (A). The lysis front position is shown in (B) at 20, 30, and 60 min under conditions of lysis described in Fig. 1.

reperfusion. After lytic breakthrough, the simulation became semiquantitative, in that it does not take into account a parabolic fluid flow within the center of the annular clot, but rather had plug flow in the annular region. Depletion of a concentration boundary layer in the flowing blood near the porous clot surface may further slow the overall lysis rate of annular clots that remain after initial lytic breakthrough.

Large-Scale Structural Variations in Thrombi

Under certain conditions, clot may have clumps or regions of dense fiber/platelets that are aggregated tightly and hence have very low permeability. The presence of these clumps would generate inhomogeneities on a large length scale. Plasmin transport would be affected by the presence of these clumps, and Darcy's law would ensure that the plasmin would permeate around the clumps. A clot having such clumps was generated by using a random number generated to compute the location of the clumps and by using a defined Gaussian function to compute the density values in the neighborhood of the clumps. The resulting permeability distribution is shown in Fig. 7A. The lysis profiles are shown in Fig. 7B. Calculation of the plasmin concentration profiles at various times indicated that the plasmin traveled at significantly faster velocities in the regions where the permeability was uniform with little penetration into the high-density clumps. This resulted in unlysed clumps of fibrin remaining after the clot dissolved. These high-density aggregates would become embolic during thrombolytic therapy. Interestingly, the low permeation regions distal of the aggregates had attenuated lysis, whereas robust lysis proceeded in the regions lateral to the clumps. This represents a mechanism by which small aggregates may lead to the generation of large emboli.

Under certain clotting conditions, a thrombus may have thin loose layers running through it. These regions would have very high permeability. This is analogous to fractures

commonly seen in other porous media problems. Simulations of the flow through "fractured" fibrin revealed the formation of a lytic finger in the thin high porosity fractures grew rapidly and led to rapid lytic breakthrough in this fractured region (simulation not shown).

Permeation in Dissolving Thrombi

We have observed that the nature of permeating fluid flow in thrombi is governed by the initial density distribution of the fibrin. During situations of lytic fingering, the velocity field in the clot becomes quite complex. This is shown in Fig. 8 for the velocity field after 1 hr of fibrin lysis (1.0 μmol/l plasmin, $\Delta P/L$ = 50 mm Hg/cm) for an initial permeability field that was randomly distributed (31.56% maximal variation). The highest velocities were present in regions where the permeability was initially highest. This caused lytic fingers to form, which then grew preferentially because the pressure drop was highest at the tip of the lytic finger. At 1 hr, the highest velocities, as well as significant velocities in the y direction, were seen at the tip of the lytic finger.

DISCUSSION

A two-dimensional model of the reaction and transport phenomena occurring during the lysis of a blood clot demonstrated that rather small variations in the initial clot density can lead to the growth of substantial dissolution fingering and lytic breakthrough. Other mechanisms that contribute to the formation of a nonuniform lysis front were investigated, including the effect of platelet retraction and the presence of localized aggregates of dense fibrin. Model predictions were compared with experimental observations using video microscopy, and it was found that the shape of the proximal face of a fibrin clot can lead to lytic breakthrough in the center of the clot because of the enhanced pressure gradient for flow in that region. We have observed that the rate of lysis would decrease after breakthrough has been achieved owing to the reduction in pressure gradients required for flow. Lysis of residual thrombi located on the walls of the blood vessel would proceed through diffusion-driven transport and, hence, is significantly slower.

The different mechanisms by which dissolution fingers may be formed are summarized as follows: (1) *structural*—a blood clot is formed by the random aggregation of fibrin bundles under flow (these bundles are typically oriented at varying angles with varying pore diameters and hence would lead to an initial permeability field varying considerably in space); (2) *rheological*—pressure-driven permeation would lead to deformation of the proximal face of a clot resulting in enhanced velocities through the middle of the blood clot; and (3) *cellular*—platelet retraction may result in less fibrin fibers present in the middle of the clot leading to higher velocities in this region. Dissolution fingers formed by any of the above mechanisms would be additive and may contribute to early but low-grade reperfusion and enhanced potential for reocclusion. The highly thrombogenic surfaces of cannulated clots, when exposed to flowing blood, are likely prone to rethrombosis. Highly aggressive lytic regimes may also be associated with higher rates of lytic fingering. Studies have shown that higher doses of recombinant single chain tPA can lead to reduced patency rates (10,13).

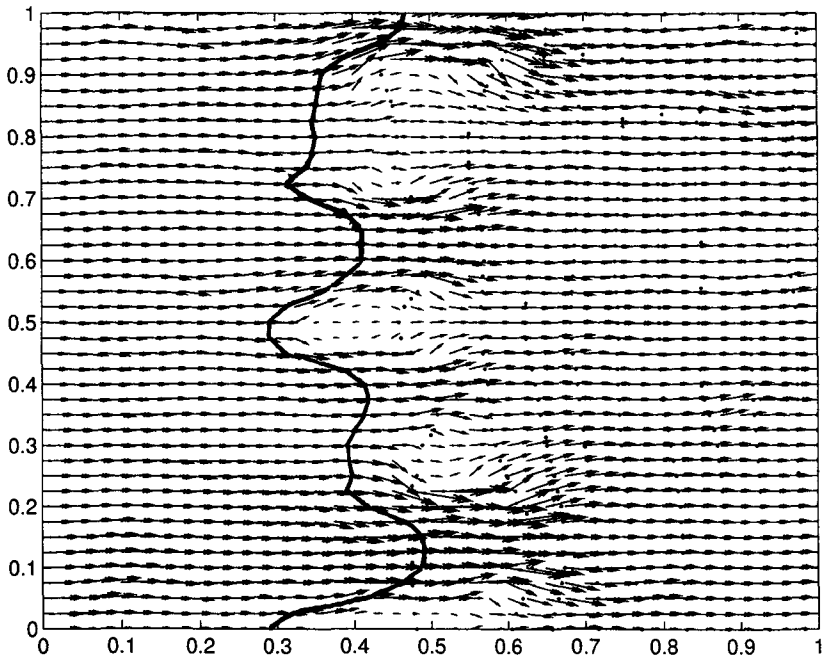

FIGURE 8. Velocity field after 60 min of lysis for fibrin containing a maximum percent variation in permeability of 31.56%. Lysis was accomplished by infusion of 1 μmol/l plasmin under the conditions described in Fig. 1. The lysis front at 50% lysis is shown as a solid line.

Recently, Zidansek *et al.* (20) have conducted a theoretical investigation using a random walk simulation of lytic fingering in two dimensions using a single characteristic reaction time required for local fibrin dissolution. Consistent with this study, our findings, which are based on a strictly continuum formulation, confirm that small random fluctuations in media properties can produce lytic fingering. Visualized by magnetic resonance imaging (20), the meandering lytic finger that moves left and right as it progresses across the retracted whole blood clot with smaller lytic fingers (directed downstream) branching from the main finger has a character consistent with the simulations of the present study. Indeed, the quantitative calculation of the local dissolution rate at the lysis front requires determination of local concentrations that depend on continual adsorption and solubilization, all of which evolve with time such that a single reaction time cannot characterize the entire process.

We have observed significant peaks in the free phase plasmin concentration at the lysis front (simulations not shown) owing to solubilization from the bound phase. It is possible that fluid recirculation regions might exist in the blood vessel upstream of the clot, especially if the clot is just distal of a bifurcation. Under these conditions, there would be mixing in regions upstream of the proximal face of the clot, and this would lead to the dissipation of the concentration peaks alluded to earlier. In light of local anatomical variations, we are evaluating the flow patterns that are formed in these regions and in future work seek to simulate these mixing effects upstream of the clot domain.

Plasmin is the only species considered in the approach presented here. In future work, we plan to extend the two-dimensional model to realistic fibrinolytic biochemistries. This will allow prediction of the shape and location of the lytic front subject to a given drug infusion scheme and local anatomical geometry. Given that the kinetic and binding properties of the various species can be altered by genetic engineering techniques, a stability analysis on the various reaction/adsorption properties of the various participating species will help predict the stability of the lytic front. Considering the nonlinear characteristics of the system, it is conceivable that certain restrictions be imposed on certain properties (biochemistry and administration) to maintain the stability of the lytic front. Experimental investigation of thrombi using magnetic resonance imaging *in vivo* or confocal microscopy *in vitro* would provide information about the random characteristics of blood clots. This data could be used with the model for enhanced predictive capability.

REFERENCES

1. Anand, S., and S. L. Diamond. Computer simulation of systemic circulation and clot lysis dynamics during thrombolytic therapy that accounts for inner clot transport and reaction. *Circulation* 94:763–774, 1996.
2. Anand, S., J. H. Wu, and S. L. Diamond. Enzyme-mediated proteolysis of fibrous biopolymers: dissolution front movement in fibrin and collagen under conditions of diffusive and convective transport. *Biotech. Bioeng.* 48:89–107, 1995.
3. Blinc A., D. Keber, G. Lahajnar, M. Stegnar, A. Zidansek, and F. Demsar. Lysing patterns of retracted blood clots with diffusion or bulk flow transport of plasma with urokinase into clots—a magnetic resonance imaging study in vitro. *Thromb. Haemost.* 68:667–671, 1992.
4. Blinc, A., G. Planinsic, D. Keber, O. Jarh, G. Lahajnar, A. Zidansek, and F. Demsar. Dependence of blood clot lysis on the mode of transport of urokinase into the clot: a magnetic resonance imaging study in vitro. *Thromb. Haemost.* 65: 549–552, 1991.
5. Blinc, A., S. D. Kennedy, R. G. Bryant, V. J. Marder, and C. W. Francis. Flow through clots determines the rate and pattern of fibrinolysis. *Thromb. Haemost.* 71:230–235, 1994.
6. Colella, P. J. Multidimensional upwind schemes for hyperbolic conservation laws. *J. Comp. Phys.* 87:171–200, 1990.
7. Diamond, S. L., and S. Anand. Inner clot diffusion and permeation during fibrinolysis. *Biophys. J.* 65:2622–2643, 1993.
8. Dullien, F. A. Porous Media: Fluid Transport and Pore Structure. New York: Academic Press, 1979.
9. Garber, P. J., A. L. Mathieson, J. Ducas, J. N. Patton, J. S. Geddes, and R. M. Prewitt. Thrombolytic therapy in cardiogenic shock: effect of increased aortic pressure and rapid tPA administration. *Can. J. Cardiol.* 11:30–36, 1995.
10. Gurbel, P. A., R. D. Anderson, C. S. Maccord, H. Scott, V. Serebruany, and W. R. Herzog. Accelerated intravenous dosing of recombinant tissue type plasminogen activator causes rapid but unstable reperfusion in a canine model of acute myocardial infarction. *Coronary Art. Dis.* 5:929–936, 1994.
11. Kincaid, D. R., and L. J. Hayes. Iterative Methods for Large Linear Systems. Boston: Academic Press, 1990.
12. LeVeque, R. J. High resolution conservative algorithms for advection in incompressible flow. *SIAM J. Numer. Anal.* 33:627–665, 1996.
13. Mueller, H. S., A. K. Rao, and S. A. Forman. TIMI Investigators. Thrombolysis in myocardial infarction (TIMI): comparative studies of coronary reperfusion and systemic fibrinolysis with two forms of recombinant tissue-type plasminogen activator. *J. Am. Coll. Cardiol.* 10:479–490, 1987.
14. Press, W. H., S. A. Teukolsky, W. T. Vetterling, and B. P. Flannery. Numerical Recipes in C: The Art of Scientific Computing (second edition). Cambridge, MA: Cambridge University Press, 1992.
15. Prewitt, R. M., S. Gu, P. J. Garber, and J. Ducas. Marked systemic hypotension depresses coronary thrombolysis induced by intracoronary administration of recombinant tissue-type plasminogen activator. *J. Am. Coll. Cardiol.* 20: 1626–1633, 1992.
16. Ranby, M., and A. Brandstorm. In: Tissue-type Plasminogen Activator (t-PA), edited by C. Kluft. Boca Raton, FL: CRC Press, 1988.
17. Strang, G. On the construction and comparison of difference schemes. *SIAM J. Numer. Anal.* 5:506–526, 1968.
18. Tiefenbrunn, A. J., R. A. Graor, A. K. Robison, F. V. Lucas, A. Hotchkiss, and B. E. Sobel. Pharmacodynamics of tissue

plasminogen activator characterized by computer-assisted simulation. *Circulation* 73:1291–1299, 1986.
19. Wu, J. H., K. Siddiqui, and S. L. Diamond. Transport phenomena and clot dissolution therapy: an experimental investigation of diffusion-controlled and permeation-enhanced fibrinolysis. *Thromb. Haemost.* 72:105–112, 1994.
20. Zidansek, A., A. Blinc, G. Lahajnar, D. Keber, and R. Blinc. Finger-like lysing patterns of blood clots. *Biophys. J.* 69: 803–809, 1995.

APPENDIX I

Meshing and Media Properties

In simulations to create variations in fibrin structure, a 11 × 11 node grid on a 1 cm × 1 cm fibrin domain was established to create 1,000 μm × 1,000 μm grid elements, each of which was assigned an initial fibrin density. This length scale of material heterogeneity was taken as one that begins to capture typical variations in real thrombi at a manageable computational cost. The computational grid for calculation of flow profiles was required to have increased resolution. Refinement of solution grids to 41 × 41 nodes provided accurate prediction of velocity profiles in the random fibrin structure. The choice of a square 1 cm × 1 cm domain facilitated the efficient use of the *nspcg* solver.

The initial fibrin density at each element can be set in a number of different ways. The fibrin density ρ may be uniform throughout the domain or have random noise fluctuations of known amplitude around a base value ρ_o at each grid element. This was achieved with a random number generator with a known seed that generates a random number R between 0 and 1 (13). For each grid element, the fibrin density was defined locally as $\rho = \rho_o + (2R - 1)$ (MPV) ρ_o, where MPV is the maximum percent variation that typically ranged from 4 to 25%. Mean percent variation of fibrin density was calculated after assignment of all elements and was about half of the maximum percent variation. For example, a domain with a maximum percent variation of 25% in the fibrin density had a mean fibrin density variation of 13.1% and an associated maximum percent variation in permeability of 86% (mean variation in permeability of 50%).

To mimic the effect of platelet retraction within a rigid vessel where the isometric tension may generate fibrin retraction away from defects within the fibrin core toward the tube periphery, we allowed the fibrin density to take on a distribution across the width of the clot, $\rho = \rho_o + (2R' - 1)$ (MPV) ρ_o, where R' is R (1 − G), G is a Gaussian function with a variance of 0.05 and an amplitude of 10, and MPV is the maximum percent variation. For material property meshes corresponding to a deformed proximal face of the clot, the fibrin density was allowed to change (hyperbolically smoothly) over three grid elements from very low levels (fluid side of the interface) to the initial fibrin level. The shape of the deformed proximal face was defined by a Gaussian curve, with maximum deflexion of 0.5 mm. To create larger length scales associated with random media heterogeneity (*i.e.*, clumps), we randomly set a number of position centers of high density around which the media was assigned a Gaussian distribution whose cross-sectional area had been randomly generated (Fig. 7A).

APPENDIX II

Staggered Grid Used for the Pressure Calculation

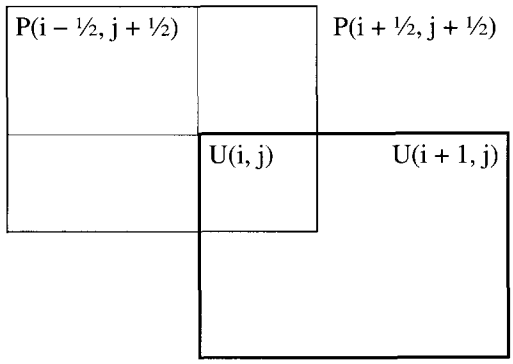

The grid used for the solution of the pressure field is indicated above. The velocity grid (indicated in **bold**) is staggered such that it lies along the midpoints of the pressure grid. Therefore, the velocity and permeability values are defined at the midpoints of the cells, whereas the pressure values are defined on the cell corners. The motivation for using a staggered grid is related to the calculation of the velocity using Darcy's law, which relates the velocity to the gradient of the pressure. The gradient of the pressure as defined above is located at the middle point of the computational cells; therefore, it is convenient to define the velocities at the midpoints.